PAPER • OPEN ACCESS

Surface properties of SnO$_2$ nanolayers prepared by spin-coating and thermal oxidation

View the article online for updates and enhancements.

IOP ebooks™

Bringing together innovative digital publishing with leading authors from the global scientific community.

Start exploring the collection−download the first chapter of every title for free.

Surface properties of SnO$_2$ nanolayers prepared by spin-coating and thermal oxidation

M Kwoka[1] , **B Lyson-Sypien**[1] , **E Comini**[2], **M Krzywiecki**[3] ,
K Waczynski[4] **and J Szuber**[1]

[1] Department of Cybernetics, Nanotechnology and Data Processing, Faculty of Automatic Control, Electronics and Computer Science, Silesian University of Technology, 44-100 Gliwice, Poland
[2] SENSOR Lab, Department of Information Engineering (DII), Brescia University, 25123 Brescia, Italy
[3] Institute of Physics—Center for Science and Education, Silesian University of Technology, 44-100 Gliwice, Poland
[4] Department of Electronics, Electrical Engineering and Microelectronics, Faculty of Automatic Control, Electronics and Computer Science, Silesian University of Technology, 44-100 Gliwice, Poland

E-mail: monika.kwoka@polsl.pl

Abstract

In this work, comparative studies of the surface morphology and surface chemistry of SnO$_2$ nanolayers prepared by spin coating with subsequent thermal oxidation (SCTO) in the temperature range of 400–700 °C using scanning electron microscopy (SEM), atomic force microscopy (AFM) and x-ray photoelectron spectroscopy (XPS) methods, are presented. The SEM images show that SCTO SnO$_2$ nanolayers contain partly connected irregular structures strongly dependent on the final oxidation temperature, with interconnected single grains of longitudinal shape and size, resulting in a flatter surface morphology with respect to the commonly used three-dimensional (3D) SnO$_2$ thin films. In turn, AFM studies additionally confirm that SCTO SnO$_2$ nanolayers after post-oxidation annealing at higher temperatures contain isolated grains of average lateral dimensions in the range of 20–50 nm having a rather flat surface morphology of average surface roughness defined by the root mean square factor at the level of ∼2 nm. From the XPS experimental research it can be concluded that, for our SCTO SnO$_2$ samples, a slight surface nonstoichiometry defined by the relative [O]/[Sn] concentration at the level of 1.8–1.9 is observed, also depending on the final post-oxidation temperature, being an evident contradiction to recently published literature using x-ray diffraction data. Moreover, XPS experiments show that there is also a permanent small amount of carbon contamination present at the surface of internal grains of our SCTO SnO$_2$ nanolayers, creating an undesired potential barrier for interactions with gaseous species when they are used as the active materials for gas sensing devices.

Keywords: tin dioxide SnO$_2$ nanolayers, spin coating technology, surface morphology, SEM, AFM, surface chemistry, XPS

(Some figures may appear in colour only in the online journal)

Introduction

Tin dioxide (SnO$_2$) is a wide band gap (3.6 eV) n-type semiconductor with a rutile structure [1] that has fascinating physicochemical properties including, among others, a high electrical conductivity ($\sim$10^2 W^{-1} × cm^{-1}) with the natural

tendency to variability after exposure to various gases [2, 3]. This is why SnO$_2$, mainly in the form of thick and thin films, has been applied in resistivity-type gas sensor devices [4, 5] for environmental and medical applications [6].

In the last decade, research has been focusing on low dimensional SnO$_2$ nanostructures, including among others nanowires and nanobelts, due to their enlarged surface-to-volume ratio as well as enhanced chemical stability and electrical performance [7, 8]. However, thin film technology is a core high-yield fabrication method for real-world sensors because of its main advantages such as low power consumption. There are various physical and chemical techniques that have been implemented recently for the preparation of SnO$_2$ thin films, which were comprehensively reviewed in [5, 6]. Depending on the deposition method, post annealing or manipulation of the substrate temperature and gas pressure can be used to control the size of the crystallites and to intentionally obtain the desired and optimized morphology. This is extremely important as the shape and size of SnO$_2$ nanostructures have a significant influence on their gas sensing properties [9, 10].

Within the physical deposition methods, a great tendency has appeared in the last several years towards developing lower temperature and inexpensive methods for deposition of SnO$_2$ nanostructured thin films. Apart from the well-known sol–gel (SG) [11] and spray pirolysis (SP) [12] methods, one of the most promising low temperature technologies for preparation of SnO$_2$ nanolayers is a method of spin coating deposition of specific precursors on Si substrate proposed by Cukrov *et al* [13] and then further developed by Bazargan *et al* [14], Khuspe *et al* [15] and Uysala *et al* [16].

Bazargan *et al* [14] recently observed that using the SnCl$_4$ solution and performing spin-coating deposition on etched glass substrates combined with post-deposition annealing (oxidation) in an oxygen atmosphere in the temperature range of 350–500 °C resulted in the formation of uniform, flat granular SnO$_2$ thin films containing monodisperse crystallites with sizes in the range of 7–10 nm and having a low root mean square (RMS) surface roughness (1.6–2.2 nm). Moreover, it was observed that after post-annealing in an oxygen atmosphere at temperatures above 500 °C the surface roughness increased since the RMS factor was evidently higher ($\sim$6), whereas the dimensions of the more isolated crystallites increased up to $\sim$25 nm.

In turn, Khuspe *et al* [15] combined the sol-gel technique for the preparation of homogeneous solution containing SnO$_2$ powder with its subsequent spin coating deposition on glass substrate for the preparation of SnO$_2$ nanostructured thin films also containing tetragonal nanocrystallites with dimensions in the range of 5–10 nm for NO$_2$ gas sensing application.

A similar sol-gel spin coating deposition procedure combined with additional post-annealing in air in the temperature range 450–650 °C was applied by Uysala *et al* [16] for the preparation of SnO$_2$ nanostructured thin films for potential photovoltaic applications.

However, it can be noticed that the issue of the local surface chemistry of SnO$_2$ nanolayers (namely the surface nonstoichiometry together with undesired carbon C contamination commonly adsorbed at the surface of various SnO$_2$ forms from the air atmosphere), has been rather neglected in the literature undertaking the subject of spin coated SnO$_2$ and listed above. This is of great importance for SnO$_2$ gas sensor performance, mainly for the gas sensitivity as well gas sensor aging effects, as observed in our recent studies of L-CVD SnO$_2$ nanolayers [17] and PVD SnO$_2$ nanowires [18].

Driven by these facts, in our last studies we have focused on the surface impact on the properties of SnO$_2$ nanolayers deposited by spin-coating and subsequent thermal oxidation (SCTO) based on the systematic comparative scanning electron microscopy (SEM) and atomic force microscopy (AFM) studies of their surface morphology, including grain dimension and roughness, combined with the x-ray photoelectron spectroscopy (XPS) studies of their surface chemistry (purity and stoichiometry) in view of their potential application in novel types of conductometric gas sensor devices.

Experimental

The SnO$_2$ nanolayers used in our studies have been deposited by the spin-coating method using SnCl$_4$·5H$_2$O in isopropanol at the rotation speed of 1800 rpm on Si(111) substrate recently cleaned (etched) in HCl solution in order to remove the natural oxide and then covered with an approximately 8 nm Au film to improve the stability, adhesion to substrate and deposited thin film homogeneity. At the second step, after a short period of drying in dry air at 100 °C, an additional thermal oxidation of the above mentioned deposited layer was performed for 1 h at various temperatures in the range of 400–700 °C in a dry air atmosphere inside a reaction chamber of a typical diffusion furnace. The thickness of our SCTO SnO$_2$ was estimated to be about $\sim$200 nm, and does not significantly evolve during above mentioned post-oxidation procedure. Other experimental details can be found in [19].

The local surface morphology of our SCTO SnO$_2$ samples was controlled using the SEM method at Brescia University (Italy), with a Zeiss LEO 1530 Model SEM microscope. More experimental details regarding this method can be found in [18]. For a more quantitative analysis of the surface morphology of our SCTO SnO$_2$ samples including the shape of individual grains, the AFM method was additionally applied using the XE-70 Park model working in a non-contact mode. In turn, the surface chemistry of SCTO SnO$_2$ thin films was controlled by the XPS method using the SPECS XPS spectrometer equipped with x-ray Al Kα source at photon energy 1486,6 eV (XR-50 model, and a concentric hemispherical analyzer (CHA PHOIBOS 100 model). Other experimental details can be found elsewhere in [17, 18].

Results and discussion

SEM and AFM investigations of SCTO SnO$_2$ thin films showed that their extremely complex morphological landscape is strongly dependent on the temperature of thermal
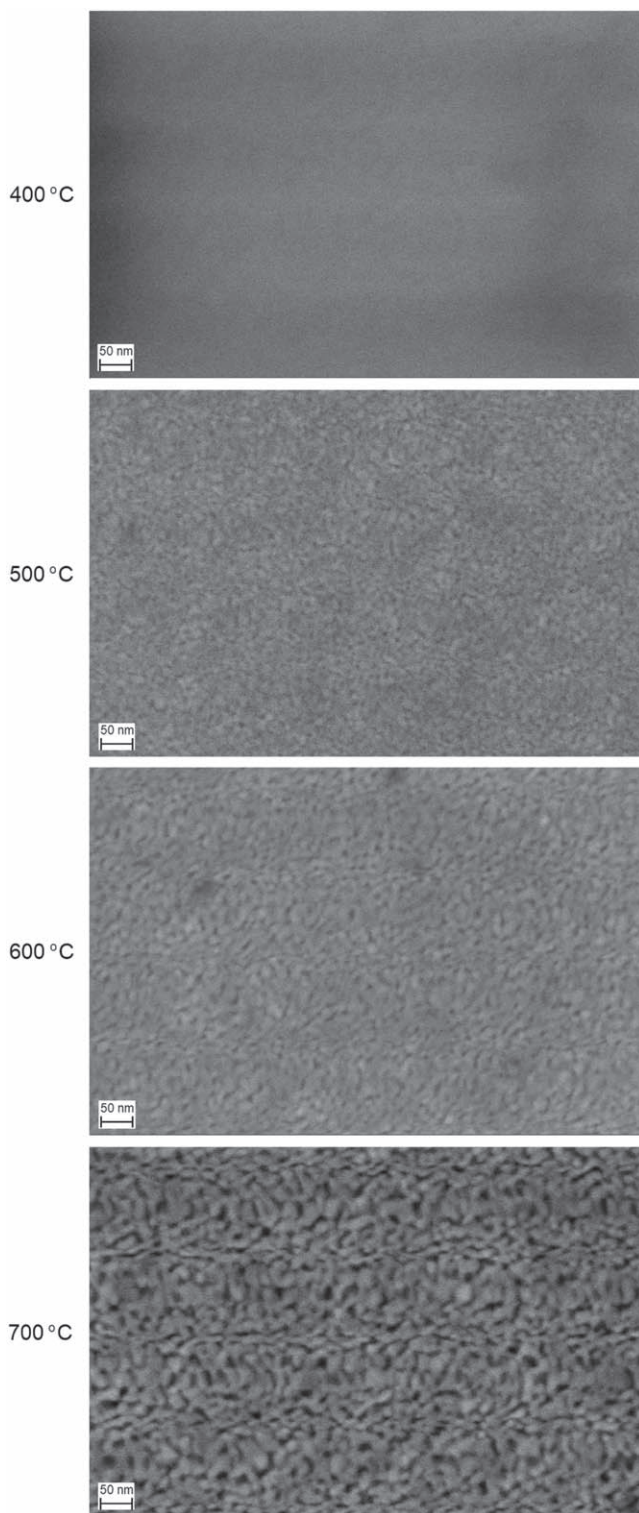
Figure 1. SEM images of SCTO SnO$_2$ nanolayers for different post-oxidation temperature in the range of 400–700 °C.

post-oxidation during the second step of the preparation procedure.

The respective SEM images of our SCTO SnO$_2$ nanolayers post-oxidized (annealed) at various temperatures in the range of 400–700 °C are shown in figure 1.

From the respective SEM images one can observe, that for the lower post-oxidation temperatures (below 500 °C) SCTO SnO$_2$ nanolayers exhibit evidently continuous surface morphology, as observed recently by Bazargan *et al* [14], without visible single crystalline forms.

What is the most important, as our SEM studies confirmed, SCTO SnO$_2$ nanolayers after post-oxidation at temperatures higher than 500 °C exhibit a well separated grain structure. In our previous paper [19], undertaking XRD phase analysis of SCTO SnO$_2$ nanolayers, it was shown that the samples demonstrated an irregular crystalline structure on the (110) facets and the Debye–Scherrer formula showed that the average sizes of the interconnected individual grain-type SnO$_2$ crystallites in the SCTO SnO$_2$ nanolayers after post-oxidation at temperatures of 500 and 700 °C were 5.1 and 6.7 nm, respectively.

In addition to the above, for the SCTO SnO$_2$ nanolayers after post-oxidation at the highest temperature of 700 °C, one can observe from the respective SEM image that the grain's shape becomes more longitudinal as the average width and length of a single grain are at the level of $\sim$20 nm and 50 nm, respectively. In relation to the above, it appears that our results of SEM characterization slightly differ from the SEM experiments of Bazargan *et al* [14], who observed almost isolated crystalline grains of the average lateral dimension $\sim$25 nm. However, there are several reasons for these differences beginning with the temperature range of the post-oxidation procedure, the various lateral resolutions of respective SEM images, different surface preparation procedures of the Si substrate, various oxidizing atmospheres of the post-oxidation procedure and finally the respective flow rates.

As was mentioned above, for additional verification of the shape of individual grains of our SCTO SnO$_2$ nanolayers, AFM comparative studies were additionally performed. Figure 2 shows the 3D AFM image of the internal, local structure of a SCTO SnO$_2$ nanolayer after post-oxidation at the highest temperature of 700 °C, together with the corresponding AFM profile.

As can be seen, the AFM experiments confirm that the nanograins of the formed SCTO SnO$_2$ nanolayers are more longitudinal with respect to the experiments of Bazargan *et al* [14] with an average maximum height below 10 nm, and average lateral dimension in the range of 20–50 nm.

However, at the same time, one can conclude that AFM imaging in the case of the presented SnO$_2$ nanolayers is moderately corrugated, which can be related to the influence of the tip convolution to a large extent. Moreover, the discussed SCTO SnO$_2$ nanolayers are rather flat as in our case the RMS factor, being the measure of the average surface roughness is at the level of $\sim$2 nm being evidently smaller ($\sim$3 times) than the one presented by Bazargan *et al* [14]. The above conclusion that our SCTO SnO$_2$ nanolayers exhibit a very flat surface morphology in comparison to the commonly used SnO$_2$ thin films, as reviewed by Eranna [7], is of great importance from the point of view of possible applications in photovoltaics as transparent conductive electrodes. Furthermore, it should be emphasized that our SCTO SnO$_2$ nanolayers after post-oxidation at
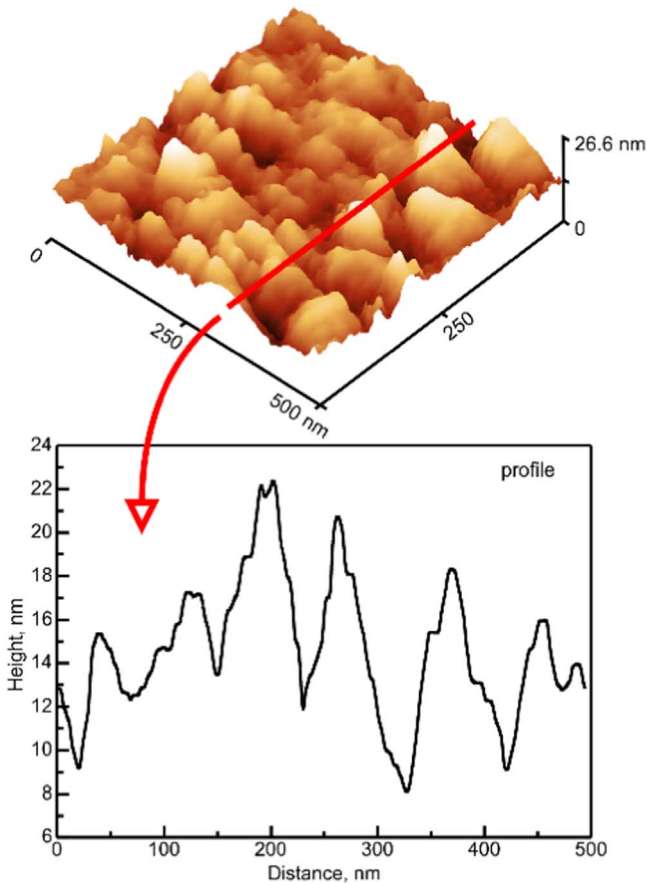
Figure 2. 3D AFM image of the internal, local structure of SCTO SnO_2 nanolayer, together with the corresponding AFM profile.
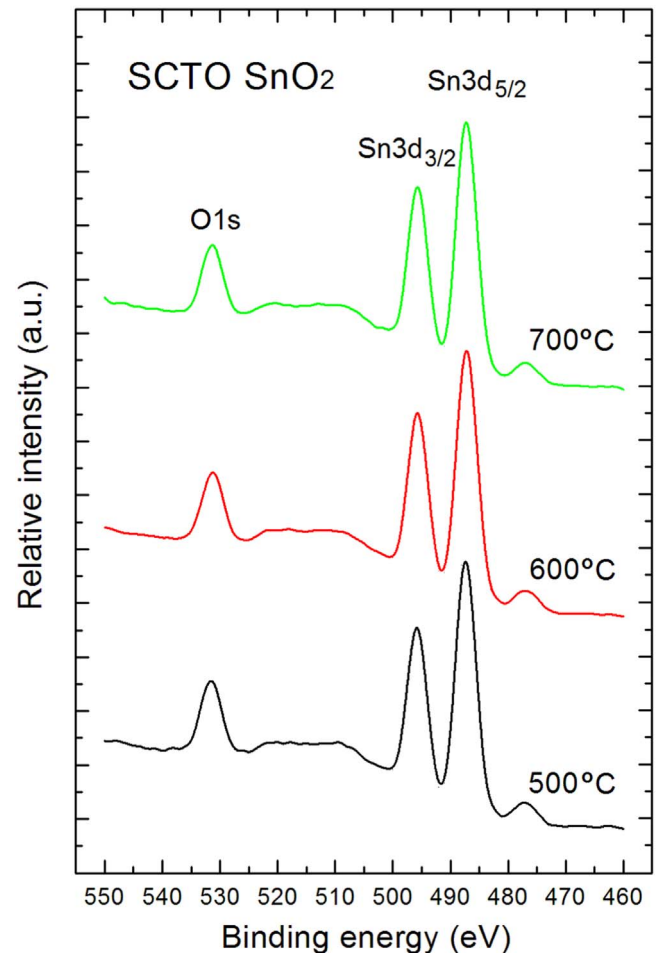

Figure 3. XPS O1s-Sn3d spectral windows of SCTO SnO_2 nanolayers for different post-oxidation temperature.

temperatures higher than 500 °C contain irregular but isolated grains of average lateral dimension not far from the Debye length ($\sim$several nm), for which the highest sensitivity of metal oxide gas sensor materials are commonly observed [7, 8]. From this point of view the SCTO SnO_2 nanolayers would be highly promising candidates for potential gas sensing applications.

In parallel to the surface morphology, in this subsection the main results of the XPS studies of SCTO SnO_2 nanolayers after deposition are presented and analyzed.

For all the XPS survey spectra of SCTO SnO_2 nanolayers for different oxidation temperatures in the rangeof 500–700 °C, which looked very similar, the contribution of the main O1s, single peaks, and the double $Sn3d_{3/2}$ and $Sn3d_{5/2}$ peaks corresponding to the two main elements were observed.

Moreover, for all XPS survey spectra, an evident contribution of single XPS C1s peak was also observed, that confirmed the existence of carbon C surface contamination on the surface of our SCTO SnO_2 nanolayers.

For a more precise analysis of the surface chemistry of our SCTO SnO_2 samples, including their stoichiometry, the core level XPS O1s-Sn3d spectral windows were used, shown in figure 3. Taking into account the area under the principal components of XPS O1s and $Sn3d_{5/2}$ peaks and using the analytical procedure based on the atomic sensitivity factor (ASF) [20], the relative [O/Sn] atomic concentration was determined. A similar procedure based on XPS survey spectra
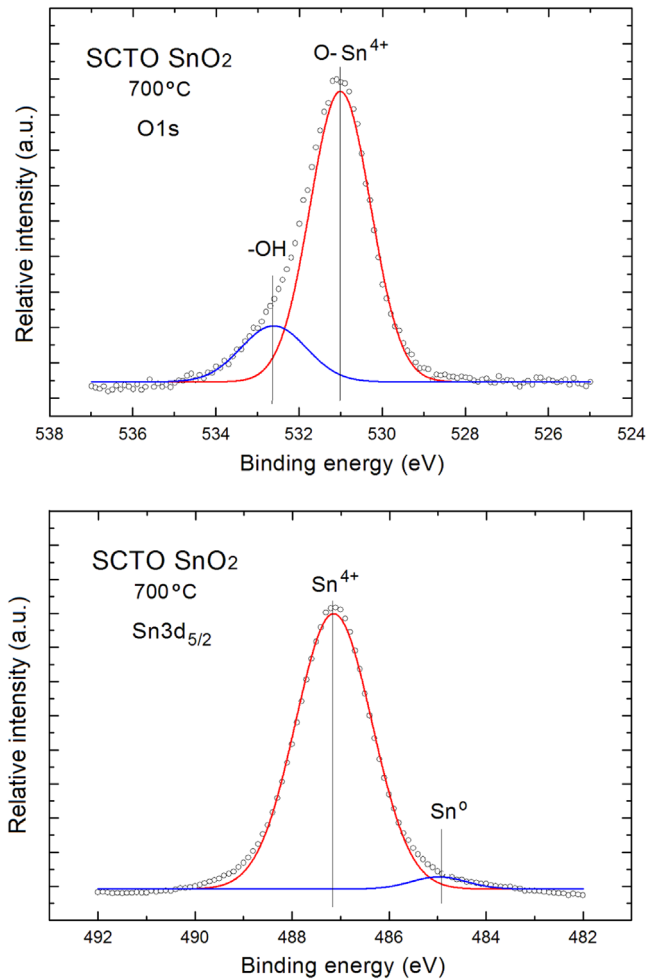
Table 1. Relative surface concentrations of O and Sn basic elements in SCTO SnO_2 nanolayers including C contamination for the different post-oxidation temperatures.

Temperature of post-oxidation of SCTO SnO_2 nanolayers [°C]	Relative concentration	
	O/Sn	C/Sn
500	1.80 ± 0.05	2.65 ± 0.08
600	1.85 ± 0.05	1.90 ± 0.08
700	1.90 ± 0.05	1.00 ± 0.08

in the binding energy range of 600–0 eV (not presented here) and the area under the respective principal components of C1s and $Sn3d_{5/2}$ was used in the determination of relative [C/Sn] atomic concentration. The obtained results for all our SCTO SnO_2 samples are summarized in table 1.

As shown in table 1, the XPS experiments confirm that the surface of all our SCTO SnO_2 nanolayers is slightly non-stoichiometric, with an evident domination of tin dioxide which is crucial, and we have to underline at this point, is that the above conclusion cannot be understood as contradictory to information obtained from our previous XRD experiments [19].

Figure 4. Decomposed XPS O1s and Sn3d$_{5/2}$ peaks of SCTO SnO$_2$ nanolayers having the highest [O]/[Sn] relative concentration.

Table 2. The binding energy, full width at half maximum (FWHM) and relative surface area of main components of XPS Sn3d$_{5/2}$ and O1s peaks after their decomposition for SCTO SnO$_2$ nanolayers.

XPS peak parameters Components	O1s		Sn 3d$_{5/2}$	
	OH–	O–Sn^{4+}	Sn^o	Sn^{4+}
Binding energy [eV]	532.4	531.0	485.0	487.2
FWHM [eV]	2.21	1.43	1.12	1.56
Relative surface area	0.36	0.64	0.04	0.96

corresponding to O atoms (ions) in bonding with various surface atoms (ions). The main parameters used in the applied fitting procedure, as well as the obtained best fitting parameters are summarized in table 2.
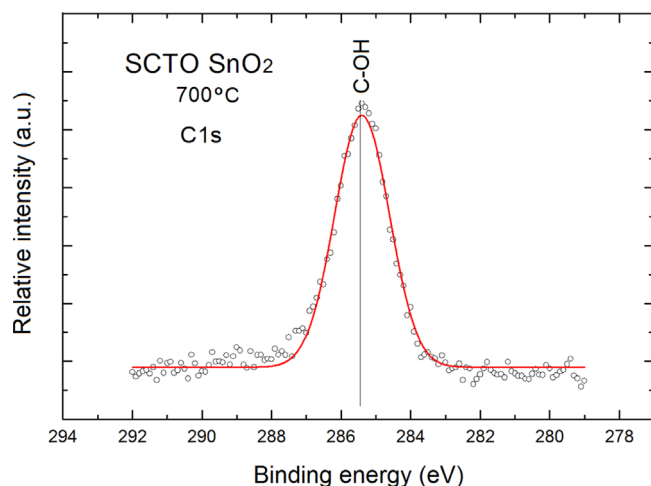
The XPS O1s line component at lower binding energy (531.0 eV) corresponds to O$_2$ ions in the Sn–O band (named lattice oxygen), whereas the second one at higher binding energy (532.4 eV) can be attributed to hydroxyl groups (H–O band) adsorbed at the surface. Their relative area (intensity) is at the level of ∼1.8. This is important, similar XPS O1s line components were recently observed by Mazloom *et al* [21] for Co-doped SnO$_2$ thin films, also prepared using the sol–gel spin coating technique.

Concerning the XPS Sn3d$_{5/2}$ line (figure 4), a simple visual shape analysis also confirms that it is wide, slightly asymmetrical and exhibits a small shoulder at the lower binding energy side of the spectrum. After decomposition (deconvolution) using fitting with Gaussian distributions, it is evident that it contains two components separated by 2.3 eV corresponding to Sn atoms (ions) bonding with various surface atoms (ions). The main parameters used in the fitting procedure, as well as the obtained fitting parameters are also summarized in table 2.

The main component of XPS Sn3d$_{5/2}$ line at higher binding energy of 471.2 eV corresponds to Sn^{4+} ions in Sn–O band (lattice oxygen), whereas the second one (very small) at lower binding energy (∼485.0 eV) can be attributed to the existence of Sn^o bondings related to the small amount of metallic Sn. Their relative area (intensity) is in good agreement with the information on relative concentration [O]/[Sn] ratios obtained from the O1s-Sn3d spectral windows that the SCTO SnO$_2$ nanolayers under the last analysis are only slightly nonstoichiometric, with an evident domination of tin dioxide SnO$_2$. Similar XPS O1s line components were also observed in our recent studies of RGVO SnO$_2$ nanolayers [22].

As was mentioned earlier, the main difference in the surface chemistry of our SCTO SnO$_2$ nanolayers, observed in the XPS survey spectra, is the amount of C contaminations.

In general, they come from the different C gaseous species present in the natural air atmosphere, which immediately adsorb at the surface of all semiconductor materials (time ∼ms) and are controlled by the mass spectrometry (MS). The relative [C]/[Sn] concentration at the surface of our SCTO SnO$_2$ nanolayers evidently depends on the post-oxidation temperature, as summarized in table 1.

The XRD results presented in [19] clearly indicated only the presence of SnO$_2$ formed in the SCTO SnO$_2$ nanolayers under study. However, in contrast to the XRD method, one has to bear in mind that XPS is primarily a surface sensitive technique, especially when using the x-ray photon energy (1486.6 eV), able to recognize the surface chemical species in the very first few layers in depth only up to 10 nm. This is why the XPS method was used in our studies for the determination of effective surface nonstoichiometry of SCTO SnO$_2$ nanolayers, which is extremely important regarding the value of the Debye length for SnO$_2$ at the level of several nm [5, 7].

In order to prove the above statement, the decomposition of XPS O1s and Sn3d$_{5/2}$ peaks for the sample with the highest [O]/[Sn] relative concentration was performed, as can be seen in figure 4.

Concerning the XPS O1s line (figure 4), a simple visual shape confirms that it is wide, asymmetrical and exhibits an evident shoulder at the higher binding energy side of the spectrum. After decomposition (deconvolution) using the fitting procedure with the Gaussian distributions, it becomes evident that it contains two components separated by 1.4 eV

Figure 5. Decomposed XPS C1s peak of SCTO SnO$_2$ nanolayers.

For the samples after post-oxidation at the lowest temperature of 500 °C it is at the level of 2.65, slightly lower than for the freshly deposited L-CVD SnO$_2$ thin films after air exposure observed in our recent studies [23–25]. In turn, for the SCTO SnO$_2$ nanolayers after post-oxidation at the highest temperature of 700 °C it is almost three times lower. This is probably related to the fact that they exhibit more tight (packaged) surface morphology corresponding to the greater dimensions of the interconnected individual nanograins and then the respective smaller channels between them are usually 'open' for potential undesired diffusion of C contaminations (mainly as CO$_2$) from the residual gas atmosphere. Crucially, the average distances between the nanograins in our SCTO SnO$_2$ nanolayers are evidently smaller with respect to the most 'open' surface observed for the L-CVD SnO$_2$ thin films, as well as the SnO$_2$ thin films obtained by the rheotaxial growth and thermal oxidation (RGTO) in our recent studies [26]. Importantly, those C contaminations at the surface of our SCTO SnO$_2$ nanolayers are in the form of C–OH bonding, as it was recognized after decomposition of XPS C1s peak shown in figure 5.

The same shape of this XPS C1s peak was observed for all the samples under our studies.

Already a simple visual shape analysis also confirms that it is wide and symmetrical.

After decomposition (deconvolution) of the XPS C1s peak using fitting with Gaussian distributions, it is evident that it contains only one component at the binding energy 285.5 eV, that can be attributed to the C-OH surface bonding commonly observed at various semiconductor surfaces including oxides [1, 20, 27]. Unfortunately, the undesired fast C adsorption on the surface of SnO$_2$ nanolayers (grains) is extremely critical for their gas sensor application because it strongly affects the response time of gas sensor devices. This is because every active (toxic) gas has to flow towards the gas sensitive active centers, for instance SnO$_2$ nanolayers, through the C contamination (up to ~3 atomic layers in average), which generates an undesired and uncontrolled barrier for potential toxic gas adsorption at the internal surface of the sensor material.

Conclusions

In this paper the results of comparative studies of the surface morphology and surface chemistry of SCTO SnO$_2$ nanolayers using a combination of SEM, AFM and XPS methods are presented. SEM and AFM studies show that the specific surface morphology of SCTO SnO$_2$ nanolayers exhibit partly connected irregular structures with interconnected single grains of more longitudinal shape and size, resulting in flatter morphology corresponding to an average roughness (RMS) below 2 nm, as derived from the AFM studies, being very promising for their potential photovoltaic applications as transparent conductive electrodes. Moreover, SCTO SnO$_2$ thin films contain almost isolated longitudinal grains of average width and length at the level of ~20 nm and 50 nm, respectively, not so far from the Debye length (~several nm). From this point of view, they can be considered as a promising novel form of metal oxide material for potential applications in novel types of conductometric gas sensors.

In turn, XPS studies confirm that for SCTO SnO$_2$ samples, a slight surface nonstoichiometry at the level of 1.8–1.9 is observed, together with C contamination, probably at the surface of internal grains. This undesired effect cannot be ignored because it generates an uncontrolled barrier for the potential adsorption of interacting gases at the internal surface of the sensor material. This is why, this undesired and uncontrolled C contamination at the internal surface of SCTO SnO$_2$ thin films appears to be the most important limitation for application in novel sensor devices. In relation to this, an understanding of the adsorption/desorption behavior of C contamination at the surface of SCTO SnO$_2$ nanolayers is crucial for the interpretation of the gas sensing mechanism. Such studies, also in comparison to the various 1D forms of SnO$_2$, including nanowires and nanobelts, are currently in progress in our labs.

ORCID iDs

M Kwoka ⬤ https://orcid.org/0000-0001-6197-1191
B Lyson-Sypien ⬤ https://orcid.org/0000-0001-6019-7835
M Krzywiecki ⬤ https://orcid.org/0000-0002-6151-8810
J Szuber ⬤ https://orcid.org/0000-0002-7012-8224

References

[1] Batzill M and Diebold U 2005 *Prog. Surf. Sci.* **79** 47
[2] Göpel W and Schierbaum K-D 1995 *Sensors and Actuators* B **26** 27
[3] Barsan N, Schweitzer-Barberich M and Göpel W 1999 *J. Anal. Chem.* **365** 287
[4] Ihokura K and Watson J 1994 *The Stannic Oxide Gas Sensor: Principles and Applications* (Boca Raton USA: CRC Press)
[5] Comini E *et al* (ed) 2009 Electrical based gas sensors *Solid State Gas Sensing* (New York: Springer) p 47
[6] Barsan N, Koziej D and Weimar U 2007 *Sensors and Actuators* B **121** 18
[7] Eranna G 2012 *Metal Oxide Nanostructures as Gas Sensing Devices* (Boca Raton USA: CRC Press)
[8] Carpenter M A, Mathur S and Kolmakov A 2012 *Metal Oxide Nanomaterials for Chemical Sensors* (New York USA: Springer)
[9] Yamazoe N 1991 *Sensors and Actuators* B **5** 7
[10] Bose C, Thangadurai P and Ramasamy S 2006 *Materials Chemistry and Physics* **95** 72
[11] Shukla S, Patil S, Kuiry S C, Rahman Z, Du T, Ludwig L, Parish C and Seal S 2003 *Sensors and Actuators* **B96** 343
[12] Brinzari V, Korotcenkov G and Golovanov V 2001 *Thin Solid Films* **391** 167
[13] Cukrov I M, Mc Cormick P G, Galatsis K and Wlodarski W 2001 *Sensors and Actuators* B **77** 491
[14] Bazargan S, Heinig N F, Pradhan D and Leung K T 2011 *Cryst. Growth Design* **11** 247
[15] Khuspe G D, Sakhare R D, Navale S T, Chougule M A, Kolekar Y D, Mulik R N, Pawar R C, Lee C S and Patil V B 2013 *Ceramics Int.* **39** 8673
[16] Uysala B Ö, Özlem Ü and Arıer A 2015 *Applied Surface Science* **350** 74
[17] Kwoka M, Ottaviano L, Koscielniak P and Szuber J 2014 *Nanoscale Research Letters* **9** 260
[18] Sitarz M, Kwoka M, Comini E, Zappa D and Szuber J 2014 *Nanoscale Research Letters* **9** 43
[19] Izydorczyk W, Waczynski K, Izydorczyk J, Karasinski P, Mazurkiewicz J, Magnuski M, Uljanow J, Waczynska-Niemiec N and Filipowski W 2014 *Materials Science (Poland)* **32** 729
[20] Moulder J F, Stickle W F, Sool P E and Bomben K D 1992 *Handbook of X-ray Photoelectron Spectroscopy* (USA: Perkin-Elmer Eden Prairie)
[21] Mazloom J and Ghodsi F E 2013 *Materials Research Bulletin* **48** 1468
[22] Kwoka M and Krzywiecki M 2015 *Materials Letters* **154** 1
[23] Kwoka M, Ottaviano L, Passacantando M, Santucci S, Czempik and Szuber J 2005 *Thin Solid Films* **490** 36
[24] Kwoka M, Ottaviano L, Passacantando M, Santucci S and Szuber J 2006 *Applied Surface Science* **252** 7730
[25] Kwoka M, Waczynska N, Kościelniak P, Sitarz M and Szuber J 2011 *Thin Solid Films* **520** 913
[26] Ottaviano L, Kwoka M, Bisti F, Parisse P, Grossi V, Santucci S and Szuber J 2009 *Thin Solid Films* **517** 6161
[27] Atashbar M Z, Sun H T, Gong B, Wlodarski W and Lamb R 1998 *Thin Solid Films* **326** 238